

Numerical Investigation of a High-Capacity Vertical Submersible Two-Stage Pump and Realization of an Experimental Test Bench for Determining the Strains and the Stresses on a Pump Shaft

Patrick Zito Malonda and Guyh Dituba Ngoma
*University of Quebec in Abitibi-Témiscamingue, School of Engineering 445,
Boulevard de l'Université, Rouyn-Noranda, Quebec, J9X 5E4, Canada*

Keywords: Vertical Submersible Pump, Axial and Radial Forces, Strain, Stress, CFX.

Abstract: A vertical submersible two-stage pump is investigated in terms of the axial and the radial forces on its shaft due to the liquid flow through the pump while accounting for the different flow rates. Also, a preliminary experimental test bench is performed to achieve the strains and the stresses on a pump shaft supporting an impeller as a function of the rotating speed. In fact, from an existing vertical submersible two-stage pump, a pump model is developed. The continuity and the Navier-Stokes equations are applied to obtain by means of the ANSYS-codes the fields of the liquid flow velocity and the pressure, as well as the axial and the radial forces acting on the pump shaft. The numerical results obtained for the pump head are validated using the experimental results. Three available axial forces for three flow rates from industry are used for the comparison with the numerical axial forces. The achieved experimental results from the preliminary test bench reveal that the strains and the stresses on the pump shaft increase with the raising of the rotating speed.

1 INTRODUCTION

The high-capacity submersible pumps are used extensively in numerous industrial, mining applications and in the mining sites in construction for the dewatering and the control of the water level.

The working of these pumps implies a strong mechanical load on the shaft and its bearings. Thus, the design process is a big challenge due to the pump performances to reach. The knowledge of all essential parameters of the components of the pump as the diameter, the width of the blades, the angles of the blades, the thickness of the blades of the impeller and the diffusers is primordial to assure an optimal manufacture of pumps (Mbock Singock, 2018). Indeed, the relative complexity to the analysis of the fluid flows through the submersible pump leads to the use of the numerical tools in the goal to determine the performances of pump notably the head, the brake horsepower and the efficiency, but also forces applied on the shaft for a good dimensionality of the bearings. This is how in the setting of this research, as long-term goals, it is about developing reliable and precise numerical approaches to determine the axial and radial forces, the strains and the stresses on the pump

shaft. The use of these approaches in the design of the submersible pumps permits to improve the performances of these pumps more while increasing reliability and the life span of the plain bearings and/or antifriction bearings of the pump shaft (FLYGT, 2004). Moreover, the literature review related to this research is stated as follows:

a) Axial and radial loads in the centrifugal pumps and the submersible pumps.

The pump manufacturers are confronted to problems of unbalance of the axial and the radial loads on the impeller because of the distribution of the static pressure on the impeller shrouds. In the case of a submersible pump, the radial force doesn't modify the good working of the pump appreciably whereas the axial force influences considerably on the working of the pump (Takacs, 2017). The use of an axial thrust bearing is ideal for the balancing of the axial force in the single-stage pumps and at low rotating speeds. Of the methods as balancing holes and the radial blades can be used to reduce force acting on the impeller rear shroud (Smith, 2005; Wilk, 2009; Dong, 2018). In the multi-stage pumps, considering the complexity of the calculation of the axial force from the distribution of the pressure on the

impeller, the dimensionality of the device of balancing of the axial force and the thrust bearing is often defined on the basis of the values by force measured at the time of the tests of the pump (Termomeccanica Pompe, 2003). The design of the volute has an influence on the radial force. This last is minimal to the point of working of the pump for a volute of simple design. The inverse occurs for a circular volute with a maximal force to the point of good working whereas a volute to double partition generates an appreciably uniform force (Badr et al., 2015).

b) Strains and stresses in the centrifugal pumps and the submersible pumps.

In practice, the regions of stress concentration are caused by grooves, keyways and cracks that entail an increase of the stresses in the pieces. At the time of the pump operating, the impellers in rotation transmit the mechanical work of the driving machine to the fluid. So the pressure load of the fluid and the inertia load due to the rotating speed induce some stresses on these impellers. The fluid pressure introduces a stress and a maximal strain more important than the one due to the inertia force. But with the increase of the thickness of the blades, the stress and the maximal strain caused by the load of the inertia force grow progressively, while the one of the load of the fluid pressure decreases (Wang et al., 2014). It agrees to underline that the raise of the diameter of the impeller also increases the stress and the strain in a centrifugal pump (Matlakala et al., 2019).

c) Plain bearings and antifriction bearings in the centrifugal pumps and the submersible pumps.

The adequate choice of the bearings depends on the dynamic behavior of the shaft, of the rotating speed and the factors as the bearing positions and the pump applications (Termomeccanica Pompe, 2003; FLYGT, 2004; Bolade et al., 2015). During the pump operating; the bearings take in charge the axial displacement and the lateral deviation of the shaft. The capacity of the bearing to function correctly is damaged by wear, fatigue or the deterioration of the lubricant. The penetration of particles in a bearing also entails the elevated stresses and a premature rupture by fatigue. These particles also produce a wear reducing the life span of the bearing (FLYGT, 2004). In a centrifugal pump, a thrust bearing must be used to balance the axial force completely in all working conditions (Badr et al., 2015).

2 MODEL DESCRIPTION

The model of the vertical submersible two-stage pump considered in this research is illustrated in Figure 1 by the solid and the fluid models. It is composed, inter alia, of a shaft, two impellers, two diffusers and a volute.

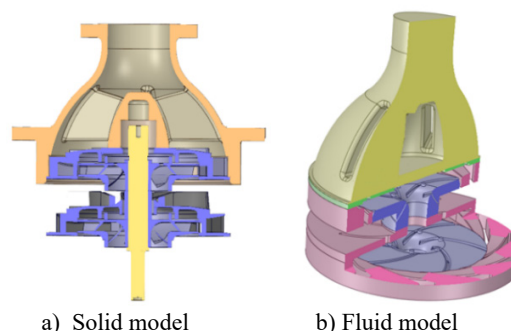


Figure 1: Vertical submersible two-stage pump.

3 MATHEMATICAL FORMULATION

To determinate the field of the liquid flow velocity, the field of the pressure, the stress and the strain in a vertical submersible two-stage pump, the following hypotheses are considered for the liquid flow (La Roche-Carrier et al., 2013; Malonda et al., 2023), and the solid mechanics (Popov, 1999): (a) a steady state, three-dimensional and turbulence flow using the $k-\epsilon$ model is assumed; (b) the liquid is an incompressible liquid; (c) it is a Newtonian liquid; and (d) the liquid's thermophysical properties are constant with the temperature; (e) the material is considered continuous, doesn't have cracks, nor cavities; (f) the material is homogeneous and presents the same properties in all points; (g) the material is considered as isotropic; and (h) no internal force acts in the material before the application of the external loads.

3.1 Liquid Flow Velocity and Pressure

The equations of the continuity and the Navier-Stokes are used to obtain the fields of liquid flow velocity and pressure. These equations are solved by means of the ANSYS CFX-code (ANSYS inc.). The equation of the continuity is expressed as follows:

$$\frac{\partial u}{\partial x} + \frac{\partial v}{\partial y} + \frac{\partial w}{\partial z} = 0 \quad (1)$$

where $u(x,y,z)$, $v(x,y,z)$ and $w(x,y,z)$ are the components of the liquid flow velocity $U(u,v,w)$.

Accounting for the gravity, the equations of the Navier-Stokes can be formulated by:

$$\begin{aligned} \rho \left(u \frac{\partial u}{\partial x} + v \frac{\partial u}{\partial y} + w \frac{\partial u}{\partial z} \right) &= \mu_{\text{eff}} \left(\frac{\partial^2 u}{\partial x^2} + \frac{\partial^2 u}{\partial y^2} + \frac{\partial^2 u}{\partial z^2} \right) \\ &\quad - \frac{\partial p}{\partial x} + \rho(\omega_z^2 r_x + 2\omega_z v) + \rho g_x \\ \rho \left(u \frac{\partial v}{\partial x} + v \frac{\partial v}{\partial y} + w \frac{\partial v}{\partial z} \right) &= \mu_{\text{eff}} \left(\frac{\partial^2 v}{\partial x^2} + \frac{\partial^2 v}{\partial y^2} + \frac{\partial^2 v}{\partial z^2} \right) \\ &\quad - \frac{\partial p}{\partial y} + \rho(\omega_z^2 r_y - 2\omega_z u) + \rho g_y \\ \rho \left(u \frac{\partial w}{\partial x} + v \frac{\partial w}{\partial y} + w \frac{\partial w}{\partial z} \right) &= \mu_{\text{eff}} \left(\frac{\partial^2 w}{\partial x^2} + \frac{\partial^2 w}{\partial y^2} + \frac{\partial^2 w}{\partial z^2} \right) \\ &\quad - \frac{\partial p}{\partial z} + \rho g_z \end{aligned} \quad (2)$$

where $g(g_x, g_y, g_z)$ is the gravity acceleration, p is the pressure; ρ is the density; μ_{eff} is the effective viscosity accounting for turbulence, it is defined as $\mu_{\text{eff}} = \mu + \mu_t$. μ is the dynamic viscosity and μ_t is the turbulence viscosity. It is linked to turbulence kinetic energy k and dissipation ε (La Roche-Carrier et al., 2013).

3.2 Axial and Radial Forces

The axial and the radial forces on the impellers are determined using the ANSYS CFX-code (ANSYS inc.). These forces are illustrated in Figure 2 for a vertical submersible two-stage pump.

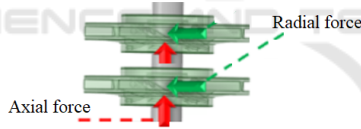


Figure 2: Axial and radial force in a model of the vertical submersible two-stage pump.

3.3 Strains and Stresses

The normal and the shear stresses on the pump shaft are determined by means of the equilibrium equations of elasticity in terms of stress neglecting the forces per unit of volume (Popov, 1999). These equations are given by:

$$\begin{aligned} \frac{\partial \sigma_x}{\partial x} + \frac{\partial \tau_{yx}}{\partial y} + \frac{\partial \tau_{zx}}{\partial z} &= 0 \\ \frac{\partial \tau_{xy}}{\partial x} + \frac{\partial \sigma_y}{\partial y} + \frac{\partial \tau_{zy}}{\partial z} &= 0 \\ \frac{\partial \tau_{xz}}{\partial x} + \frac{\partial \tau_{yz}}{\partial y} + \frac{\partial \sigma_z}{\partial z} &= 0 \end{aligned} \quad (3)$$

The normal and the shear strains are formulated as follows using the displacements (u,v,w) respectively in the directions of x , y and z

$$\begin{aligned} \varepsilon_x &= \frac{\partial u}{\partial x}; \quad \varepsilon_y = \frac{\partial v}{\partial y}; \quad \varepsilon_z = \frac{\partial w}{\partial z} \\ \gamma_{xy} &= \frac{\partial u}{\partial y} + \frac{\partial v}{\partial x}; \quad \gamma_{yz} = \frac{\partial w}{\partial z} + \frac{\partial v}{\partial z}; \quad \gamma_{zx} = \frac{\partial u}{\partial z} + \frac{\partial w}{\partial x} \end{aligned} \quad (4)$$

The relationships between the stresses and the strains is given by:

$$\begin{aligned} \sigma_x &= \frac{1}{E} [\sigma_x - \nu(\sigma_y + \sigma_z)] \\ \sigma_y &= \frac{1}{E} [\sigma_y - \nu(\sigma_z + \sigma_x)] \\ \sigma_z &= \frac{1}{E} [\sigma_z - \nu(\sigma_x + \sigma_y)] \\ \tau_{xy} &= \frac{\tau_{xy}}{G}; \quad \tau_{yz} = \frac{\tau_{yz}}{G}; \quad \tau_{zx} = \frac{\tau_{zx}}{G} \end{aligned} \quad (5)$$

where E is the modulus of elasticity, G is the shear modulus and ν is the Poisson's ratio.

The stresses can be written as a function of the strains by:

$$\begin{aligned} \sigma_x &= \frac{E}{(1+\nu)(1-2\nu)} [(1-\nu)\varepsilon_x + \nu(\varepsilon_y + \varepsilon_z)] \\ \sigma_y &= \frac{E}{(1+\nu)(1-2\nu)} [(1-\nu)\varepsilon_y + \nu(\varepsilon_z + \varepsilon_x)] \\ \sigma_z &= \frac{E}{(1+\nu)(1-2\nu)} [(1-\nu)\varepsilon_z + \nu(\varepsilon_x + \varepsilon_y)] \\ \tau_{xy} &= G\gamma_{xy}; \quad \tau_{yz} = G\gamma_{yz}; \quad \tau_{zx} = G\gamma_{zx} \end{aligned} \quad (6)$$

The stress of von Mises selected for the yield criteria can be expressed by:

$$\sigma' = \sqrt{\frac{1}{2} \left((\sigma_1 - \sigma_2)^2 + (\sigma_2 - \sigma_3)^2 + (\sigma_3 - \sigma_1)^2 \right)} \quad (7)$$

where σ_1 , σ_2 and σ_3 , are the principal stresses in the directions of 1, 2 and 3 according to $\sigma_1 > \sigma_2 > \sigma_3$ (Popov, 1999; Malonda et al., 2023).

3.4 Diffuser Equations

The diffuser equations (Gülich, J. F., 2010; Malonda et al., 2023) are applied in this research to calculate the main parameter of the diffusers of the vertical submersible two-stage pump.

4 NUMERICAL IMPLEMENTATION, SUBMERSIBLE PUMP MODELING AND SIMULATION STEPS

The differential equations of continuity and Navier-Stokes from the mathematical formulation including the model of turbulence are solved using the ANSYS-CFX module. In sum, Figure 3 illustrates the

modeling and the simulation steps for a vertical submersible two-stage pump using the Inventor and the ANSYS softwares (modules: Spaceclaim, CFX-Pre, CFX-Solver and CFX-Post) and accounting for the boundary conditions. The frozen-rotor is used to take into account the rotating impeller.

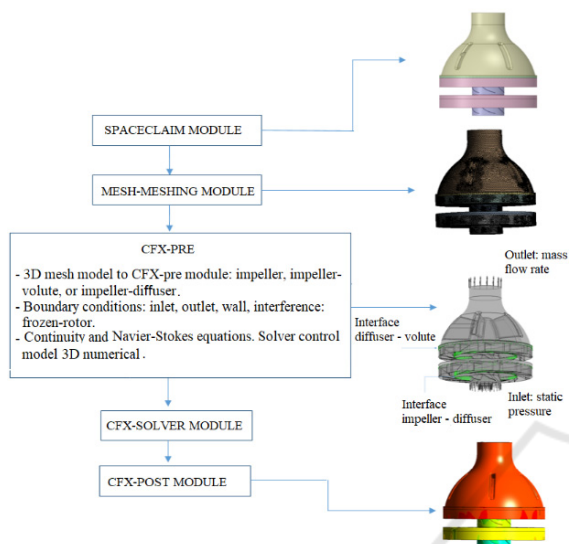


Figure 3: Modeling of the reference vertical submersible two-stage pump et simulation steps.

5 RESULTS AND DISCUSSION

The numerical simulations are done applying the reference data for the water, the pump shaft, the impeller, and the diffuser according to the Tables 1-5.

Table 1: Properties of water in 25 °C.

Density [kg/m ³]	Thermal expansion coefficient [K ⁻¹]	Kinematic viscosity [m ² /s]
997	2,57x10 ⁻¹	0,884x10 ⁻⁶

Table 2: Properties of the 17-4PH steel for the shaft.

Module of the Young [Pa]	1,96x10 ¹¹
Poisson ratio	0,3
Compressibility module [Pa]	1,63x10 ¹¹
Shear module [Pa]	7,53x10 ¹⁰
Resistance coefficient [Pa]	9,2x10 ⁸
Ductility coefficient [Pa]	10 ⁹
Yield strength [Pa]	7.93x10 ⁸
Ultimate tensile strength [Pa]	1.103x10 ⁹
Density [kg/m ³]	7750,4

Table 3: Impeller data.

Inlet blade height b ₁ [mm]	30.17
Outlet blade height b ₂ [mm]	14.48
Hub diameter D _{h1} [mm]	44,45
Inlet diameter D _{h2} [mm]	107.95
Outlet diameter D ₂ [mm]	241
Inlet blade angle β _{b1} [°]	16
Outlet blade angle β _{b2} [°]	27.5
Blade thickness e [mm]	3.17
Blade number Z _b	7

Table 4: Diffuser (front side) data.

Inlet blade height b ₃ [mm]	17.46
Outlet blade height b ₄ [mm]	40.64
Inlet diameter D ₃ [mm]	243,84
Outlet diameter D ₄ [mm]	311.15
Inlet blade angle α _{3b} [°]	10
Blade thickness e ₃ [mm]	3.175
Blade number Z _{Le}	8

Table 5: Diffuser (rear side) data.

Return vane number Z _R	6
Outlet return vane height b ₅ [mm]	24,4
Diameter at the inlet of the return vane D ₃ [mm]	311,15
Blade angle at the inlet of the return vane α ₅ [°]	95
Blade angle at the outlet of the return vane α ₆ [°]	18
Blade thickness of the return vane e ₃ [mm]	6,04

Moreover, four case studies are accomplished: a) the characterization and the validation of the developed vertical submersible two-stage pump; b) the effect of the axial and the radial loads as a function of the flow rate; c) the result comparison in terms of the axial forces; d) the variation of the strain and the stress on the pump shaft as a function of the rotating speed.

The numerical simulation results presented in this research are obtained with the highest accuracy by conducting mesh-independent solution tests in each case study using different numbers of mesh elements.

5.1 Numerical Characterization and Validation of the Model Vertical Submersible Two-Stage Pump

To numerical characterize the developed pump model in terms of pump head using the water flow, the flow

rate range from 492.192 m³/h to 533.196 m³/h are selected keeping the other parameters constant.

Figure 4 represents the numerical curve and the experimental curve of pump head as a function of the flow rate. It is observed a good agreement between both curves. The corresponding relative deviations in absolute value of the comparison results as a function of the flow rate are illustrated in Figure 5. It can be seen that the relative gaps (R_g) are lower than 5% for the considered flow rates. Thus, the pump model can predict the hydraulic performances of the pump.

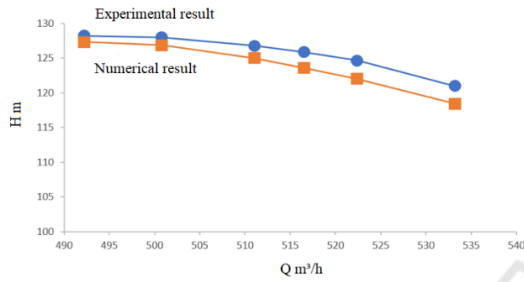


Figure 4: Pump head versus flow rate.

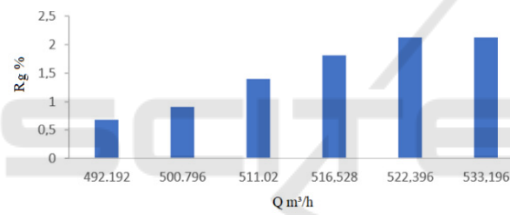


Figure 5: Relative gap of the pump head versus flow rate.

5.2 Effect of the Flow Rate on the Axial and the Radial Forces

The analysis of the stresses and the strains is achieved by means of the solid model while integrating the internal pressures of the impellers, the axial and the radial forces and the torques obtained from the simulations of the fluid model according to the flow rate and the rotating speed of the pump.

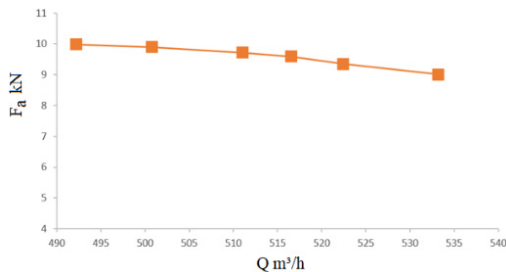


Figure 6: Axial force versus flow rate.

Figures 6 and 7 illustrate the axial and the radial forces according to the conditions of working in terms of flow rate and rotating speed. In these figures, it is observed that the axial and the radial forces on the impellers decreases slightly when the flow rate increases.

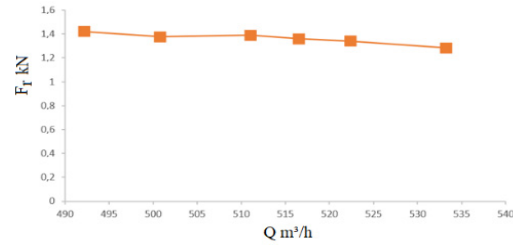


Figure 7: Radial force versus flow rate.

5.3 Axial Force Validation for Three Flow Rates

The comparison between the only three axial forces obtained from the pump manufacturer corresponding to three flow rates and the numerical results is indicated in Table 6 including the relative gaps.

Table 6: Axial forces for three flow rates.

Flow rate [m ³ /h]	Numerical result [N]	Industrial result [N]	Relative gap [%]
114	10115.28	9388	7.1
511	9758.65	9277	4.9
681	7915.51	7581	4.2

5.4 Experimental Results





5.4.1 Test Bench

The developed experimental test bench is preliminary for obtaining the strains and the stresses on the pump shaft. It is composed of an impeller, a shaft, two bearings and an electric motor. Table 7 shows the main elements of the test bench (School of Engineering). It is to highlight that this research will be completed (future work) designing an experimental test bench for the strain, the stress, the axial and radial forces using an existing submersible vertical two-stage pump in operating.

Furthermore, the different steps to achieve the installation of the Wiser 1 data acquisition system on the shaft are the following (Figures 8 and 9):

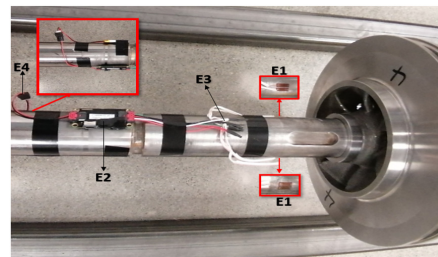
- Step 1 (E1): To install the strain gauges on the shaft and the wire in a complete bridge. As the maximal concentration zone is on the impeller keyway, the strain gauges will be placed near of this zone.

Table 7: Test bench elements.

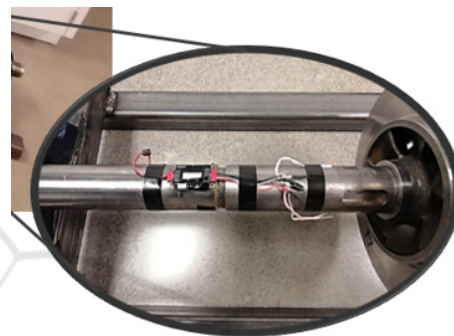
Element	
Tecat (Wiser 1) data acquisition system	
CC-33Ax5 strain gauge	
TPS 2024 oscilloscope Tektronix	
ATV312 Variable speed drive	

- Step 2 (E2): To bring up the remote transmitter and the battery, close to the strain gauges.
- Step 3 (E3): To use the cable to strain gauges included to connect the remote transmitter unit in the circuit of the bridge to strain gauges.
- Step 4 (E4): To use the included battery cable to connect the battery to the remote transmitter unit.
- Step 5 (E5): To connect the antenna included to the basis receiver and the unit supply of the basis receiver in 12-24V DC via a jack plug connector or 5V via a micro-USB connector.
- Step 6 (E6): If the basis receiver is within reach of the distant system and that this last is supplied by a battery, the unit of basis will establish a RF connection within 10 seconds about.
- Step 7 (E7): Once the established cordless connection, the blue LED placed in the front of the basis unit must become blue stationary. If it is the case, the basis unit actively gives out the signals that it received from the remote control on the four analog 0-5V output channels.

- Step 8 (E8): The analog 0-5V output of the stress signal must be connected to a data acquirement system to record the signal of tension.



a)



b)

Figure 8: Installation of the Wiser 1 data acquisition system on the pump shaft supporting impeller.

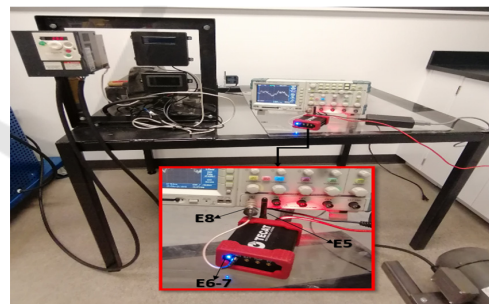


Figure 9: Connecting the transceiver of the Wiser 1 data acquisition system.

5.4.2 Effect of the Rotating Speed on the Strain and the Stress

Figures 10 and 11 illustrate the strain (ϵ) and the stress (σ') on the shaft according to the rotating speed with the strain gauges placed as indicated on Figure 8. It can be seen that the strain and the stress increase with the augmentation of the rotating speed increases.

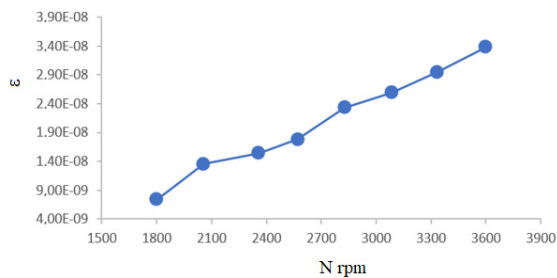


Figure 10: Strain versus rotating speed.

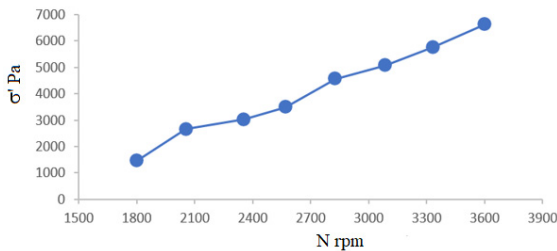


Figure 11: Stress versus rotating speed.

6 CONCLUSIONS

In this study, a submersible vertical two-stage pump is numerically investigated in terms of the induced axial and radial forces, and a preliminary test bench was realized for determining the strains and the stresses on a pump shaft with an impeller. From an existing vertical submersible two-stage pump, a numerical pump model is developed. The ANSYS-CFX is used for the resolution of the continuity and the Navier-Stokes equations and the simulations. A good agreement is achieved between the numerical simulation results obtained and the experimental results for the pump head. Furthermore, the numerical results of the axial force were compared with the industrial results for three different flow rates. The relative gaps from both result comparisons reveal the relevant of the developed model of the submersible vertical two-stage pump. In addition, an experimental study is done on a pump shaft. It is observed that more the rotating speed increases, more the strain and the stress on the shaft also raise. Further research work is planned to complete the experimental test bench for the strain, the stress, the axial and radial forces using an existing submersible vertical two-stage pump in operating. This will allow to develop a generalized numerical correlation for the calculations of the strain, the stress, the axial and the radial forces in the submersible vertical two-stage pumps while being based on the experimental results.

ACKNOWLEDGEMENTS

The authors are grateful to the Technosub Inc., Industrial pumps manufacturing and distribution (Rouyn-Noranda, Quebec, Canada) and the Turbomachinery laboratory of the Engineering School (University of University of Quebec in Abitibi-Témiscamingue).

REFERENCES

- Abdelouhab, M. A., Dituba Ngoma. G., Erchiqui, F., Kabeya, P. (2020). Numerical Study of the Axial and Radial Forces, the Stresses and the Strains in a High Pressure Multistage Centrifugal Pump. *10th International Conference on Simulation and Modeling Methodologies, Technologies and Applications (SIMULTECH)*.
- ANSYS inc., www.ansys.com.
- Badr, H. M., Ahmed, W. H. (2015). *Pumping machinery theory and practice*. John Wiley & Sons.
- Bolade P. S., Madki, S. J. (2015). Analysis of Hydraulic Thrusts in Centrifugal Pump to Increase the Bearing Life. *International Journal of Engineering Research & Technology (IJERT)*, Vol. 4 Issue 08.
- Dong W., Chu W. L. (2018). Numerical Investigation of the Fluid Flow Characteristics in the Hub Plate Crown of a Centrifugal Pump. *Chinese Journal of Mechanical Engineering*, vol. 31, p. 64.
- FLYGT, ITT (2004). Industries Engineered for life: Shaft and Bearings Calculations. *02.03.Eng. 0,5 M. 04.04; 892932; www.flygt.com*.
- Gulich, J. F. (2010). *Centrifugal Pumps*, second Edition, Springer.
- La Roche-Carrier N., Dituba Ngoma G., and Ghie W. (2013). Numerical investigation of a first stage of a multistage centrifugal pump: impeller, diffuser with return vanes, and casing. *ISRN Mechanical Engineering*, Vol. 2013, Article ID 578072, 15 pages.
- Malonda, P. Z., Dituba Ngoma, G., Ghié, W., Erchiqui, F., Kabeya, P., Kifumbi, F. (2023). *Performance Study of Vertical Submersible Pump in Terms of Induced Loads and Vibrations*. Lecture Notes in Networks and Systems, vol 601. Springer.
- Matlakala, M., Kallon, D., Mogapi, K., Mabelane I., Makgopa, D. (2019). Influence of Impeller Diameter on the Performance of Centrifugal pumps. *IOP Conference Series: Materials Science and Engineering*.
- Mbock Singock, T. A. (2018). Conception et caractérisation numérique d'une pompe à turbine verticale de grande capacité. Université du Québec en Abitibi-Témiscamingue.
- Popov E. P. (1999). *Engineering Mechanics of Solids, 2nd edition*, Prentice Hall.
- School of Engineering, Turbomachinery laboratory (E-216), University of Quebec in Abitibi-Témiscamingue (UQAT), www.uqat.ca.

- Smith, D. R., Price, S. (2005). Upthrust problems on multistage vertical turbine pumps. *Proceedings of the 22nd International Pump Users Symposium*.
- Takacs, G. (2017). *Electrical submersible pumps manual: design, operations, and maintenance*. Gulf professional publishing.
- Termomeccanica Pompe T.M.P. S.p.A. (2003). *TERMOMECCANICA Centrifugal pump handbook*, La Spezia - Italy.
- Wang, C., Shi, W., Si, Q., Zhou, L. (2014). Numerical calculation and finite element calculation on impeller of stainless steel multistage centrifugal pump. *Journal of Vibroengineering*, vol. 16, pp. 1723-1734.
- Wilk, A. (2009), Laboratory investigations and theoretical analysis of axial thrust problem in high rotational speed pumps. *WSEAS Trans. Fluid Mech*, vol. 4.

